



Contents lists available at ScienceDirect

## Arabian Journal of Chemistry

journal homepage: [www.ksu.edu.sa](http://www.ksu.edu.sa)

Original article



# Waste para-rubber wood ash and iron scrap for the sustainable preparation of magnetic Fenton catalyst for efficient degradation of tetracycline

Natthanan Rattanachueskul<sup>a</sup>, Parichart Onsri<sup>a</sup>, Waralee Watcharin<sup>b</sup>, Arthit Makarasen<sup>c</sup>, Supanna Techasakul<sup>c</sup>, Decha Dechtrirat<sup>c,d,e,\*</sup>, Laemthong Chuenchom<sup>a,f,\*</sup>

<sup>a</sup> Division of Physical Science, Faculty of Science, Prince of Songkla University, Songkhla 90110, Thailand

<sup>b</sup> Faculty of Biotechnology (Agro-Industry), Assumption University, Hua Mak Campus, Bangkok 10240, Thailand

<sup>c</sup> Laboratory of Organic Synthesis, Chulabhorn Research Institute, Bangkok 10210, Thailand

<sup>d</sup> Department of Materials Science, Faculty of Science, Kasetsart University, Bangkok 10900, Thailand

<sup>e</sup> Specialized Center of Rubber and Polymer Materials for Agriculture and Industry (RPM), Faculty of Science, Kasetsart University, Bangkok 10900, Thailand

<sup>f</sup> Center of Excellence for Innovation in Chemistry, Faculty of Science, Prince of Songkla University, Songkhla 90110, Thailand

## ARTICLE INFO

## Keywords:

Fenton reaction  
Zero-waste  
Iron scrap  
Para-rubber wood ash

## ABSTRACT

This study introduces a sustainable method of synthesizing a magnetic Fenton catalyst. The use of readily available iron scrap waste and para-rubber wood ash from heating and power plants is innovative and cost-effective. The catalyst is obtained from the precursor materials by pyrolysis. The physicochemical properties of the catalyst were characterized to investigate the effects of different iron-to-ash ratios and pyrolysis temperatures. The Fenton process was investigated through the degradation of tetracycline (TC). A catalyst produced with an iron-ash ratio of 1:2 exhibited exceptional performances with a TC removal rate of up to 90 % within 15 min under optimized conditions. The Fenton catalyst also possessed desirable magnetic properties, enabling easy separation. The stable catalyst could be regenerated and was successfully recycled four times while retaining its efficiency. This research not only addresses environmental concerns but also highlights the potential value of two waste materials in the synthesis of advanced Fenton-like catalysts.

## 1. Introduction

Antibiotic resistance acquired from antibiotic contamination poses a risk to aquatic ecosystems and human health (Wang & Zhuan, 2020; Xiang et al., 2020; Zhang et al., 2018). A substantial volume of antimicrobial agents is released annually into the environment, with tetracycline (TC) emerging as one of the most frequently identified antibiotic compounds within aquatic ecosystems. (Wang et al., 2021). The elimination of TC from aquatic environments by adsorption (Dutta & Mala, 2020; Krasucka et al., 2021; Priya & Radha, 2017) and coagulation (Choi et al., 2008; Saitoh et al., 2017) creates TC-contaminated solids which are considered hazardous waste. The suitable procedure for the collection and disposal of this waste has become a crucial issue since unsuitable disposal may discharge the contamination back into the environment. This issue can be addressed by the use of advanced oxidation processes, which break down organic contaminants with highly reactive radicals. These promising chemical processes offer

advantages of technical feasibility, complete mineralization, high efficiency, and the ability to operate at ambient temperatures and pressures.

One of the more familiar advanced oxidation processes is the Fenton reaction, which uses H<sub>2</sub>O<sub>2</sub> and an iron-based catalyst. Iron-based materials such as zero-valent iron (Chen et al., 2023; Jiang et al., 2020; Li et al., 2023; Yoon & Bae, 2019), iron oxides (Khataee et al., 2017; Li et al., 2022; Radoń et al., 2019; Rashmishree et al., 2023) and iron compounds (Agú et al., 2020; Soufi et al., 2021) have been extensively studied for the Fenton-like degradation of TC. Incorporating magnetic characteristics into Fenton catalysts during the preparation process is an approach that increases their applicability and facilitates the separation of catalysts. The acquired magnetic properties can be tuned to allow the rapid and effective separation of the catalyst with an external magnet and suitably magnetized iron particles can serve as active sites for Fenton-like reactions. This combination of tunable magnetic properties and catalytic functionality offers significant advantages in the field of wastewater treatment and pollutant degradation but the commercial

Peer review under responsibility of King Saud University.

\* Corresponding authors.

E-mail addresses: [fscidcd@ku.ac.th](mailto:fscidcd@ku.ac.th) (D. Dechtrirat), [laemthong.c@psu.ac.th](mailto:laemthong.c@psu.ac.th) (L. Chuenchom).

<https://doi.org/10.1016/j.arabjc.2024.105791>

Received 1 March 2024; Accepted 9 April 2024

Available online 11 April 2024

1878-5352/© 2024 The Author(s). Published by Elsevier B.V. on behalf of King Saud University. This is an open access article under the CC BY-NC-ND license (<http://creativecommons.org/licenses/by-nc-nd/4.0/>).

chemicals used as precursors increase production costs.

Alternative precursors that are less expensive than the traditional iron salts are available in abundance and could lead to a sustainable method of reducing costs. Steel, for instance, is used in large quantities in fields such as transportation, building construction and manufacturing. The large volume of steel used creates waste materials, known collectively as iron scrap, that can be recycled by smelting at high temperatures, which is a costly and energy-intensive process (Koch et al., 2002). It is, however, feasible to use iron scrap in a more economical way as a precursor for advanced, novel, composite materials (Babar et al., 2018; Chandane et al., 2019; Deganello et al., 2019; Fatimah et al., 2023; Priyadarshini et al., 2023) produced in processes that uphold the principles of sustainable chemistry.

To improve the efficiency of iron-based catalysts, many studies have attached the catalysts to solid supports such as silica (Do et al., 2018; Farhadian et al., 2021; Fatimah et al., 2019; Munoz et al., 2015; Šuligoj et al., 2023; Wang & Zhuan, 2020) and carbon-based materials (Chen et al., 2020; Li et al., 2020; Lu et al., 2023; Priyadarshini et al., 2023; Tao et al., 2023; Wang & Zhuan, 2020; Wu et al., 2024; Yoo et al., 2017). These works were motivated by the stability, low toxicity, widespread availability and cost-effectiveness of the supporting materials. Para-rubber wood ash (PRA) is the residual solid waste produced by the combustion of para-rubber wood for electricity generation in wood substitute industries (Hasan et al., 2000; Masae, 2013; Saosee et al., 2020). In Thailand, the world's major producer of para-rubber wood, this practice produces a large amount of ash (Masae, 2013), which is classed as particulate matter and causes air pollution and respiratory diseases (Le Blond et al., 2017; Rodríguez-Díaz et al., 2015). Many attempts have been made to find a use for PRA, whether as a component of building materials (Madurwar et al., 2014; Sales & Lima, 2010; Xu et al., 2018) or as an acidic soil neutralizer to increase agricultural output (Purnomo et al., 2018; Webber et al., 2017). PRA is also a promising material as a catalyst support, due to its large surface area, stability and silica-based structure (Abdul Mutalib et al., 2020; Fatimah et al., 2019; Ma et al., 2020). Therefore, iron scrap and PRA are potentially intriguing starting materials for the synthesis of a magnetic Fenton catalyst.

In this work, a magnetic PRA catalyst (MPRA) is obtained by the simple pyrolysis of PRA previously impregnated with an iron scrap solution. PRA possesses favorable chemical properties that make it a promising catalyst support for iron oxide. Notably, its inert silica surface can hinder the aggregation of magnetic particles in liquid media during synthesis, thereby enhancing stability and mitigating concerns related to biodegradability and toxicity (Thangaraj et al., 2019). At the same time, hydroxyl groups on the surface of PRA facilitate strong interactions between the support and iron oxide particles (Vinayagam et al., 2022). Additionally, synthesizing a Fenton catalyst from PRA and iron scrap not only adds value to these waste materials but also contributes to the development of sustainable catalytic processes. Harnessing these chemical advantages holds significant potential for advancing catalytic systems.

## 2. Experimental

### 2.1. Materials and chemicals

Sodium hydroxide (97.0 %) was from RCI Labscan (Bangkok, Thailand); hydrochloric acid (36.5–38.0 %) from J.T. Baker (Phillipsburg, NJ, USA); and tetracycline hydrochloride (>98.0 %) from TCI America (Portland, OR, USA). PRA was obtained from the wood substitute plant of Panel Plus Public Company Limited in Songkhla, Thailand, and was used as a catalyst support. Iron scrap was obtained from a local junkyard in Songkhla Province. Experiments were carried out with AR-grade chemicals of high purity and deionized (DI) water.

### 2.2. Preparation of MPRA catalyst

A solution of iron scrap was prepared by dissolving iron scrap in concentrated HCl (1 g/mL) under stirring for 20 min. The obtained solution was diluted with DI water at a ratio of 1:3. Various precursor mixtures were then prepared by mixing 15 g of PRA under stirring for 1 h with different amounts of iron precursor solution to give weight ratios of iron scrap–PRA of 1:1, 1:2, and 1:4. In the optimal catalyst ultimately used to impregnate PRA, 15 g of PRA were mixed with 300 mL of the diluted iron scrap solution to give an iron scrap–PRA weight ratio of 1:2 and a total iron concentration of ~ 6250 mg/L. The various mixtures were dried at 110 °C and dried samples were pyrolyzed for 1.5 h under nitrogen gas at different temperatures from 600 to 800 °C, ramped at 2 °C/min to obtain magnetic iron oxide@PRA composites (MPRA).

The obtained PRA catalysts were labeled MPRAx-y-T, where x-y represents the weight ratio of iron scrap–PRA and T is the pyrolysis temperature, and a control catalyst, denoted Scrap-800, was prepared using the same procedure without the inclusion of PRA. All prepared materials were ground to a fine powder with a particle size of around 20 μm measured by field emission scanning electron microscope (FESEM) analysis. Five replications of each sample were produced and the overall preparation yield is shown in Table S1.

### 2.3. Characterization of MPRA catalysts

The surface morphology of the particles was examined by field emission scanning electron microscopy integrated with energy-dispersive X-ray spectroscopy (FESEM-EDX, Apreo, FEI). Pore volume, pore size, and surface area were determined using a nitrogen adsorption/desorption analyzer (ASAP2460, Micromeritics). Prior to N<sub>2</sub> adsorption/desorption examination, the samples were degassed at 120 °C for 16 h. Functional groups and iron species at the surface of the catalyst were identified by Fourier transform infrared spectroscopy (FT-IR, Spectrum GX, Perkin Elmer) from 4000 to 400 cm<sup>-1</sup> utilizing a KBr pellet. Surface functionalities were quantitatively and qualitatively analyzed by X-ray photoelectron spectroscopy (XPS, AXIS Ultra DLD, Kratos Analytical Ltd.). The crystal structure and iron speciation of samples was analyzed by X-ray diffraction analysis (XRD, Philips, X'Pert MPD), with a 2θ scanning range of 5° to 90° and a step size of 0.05°. The magnetization of samples was studied at 298 K using a vibrating sample magnetometer (VSM, Lake Shore). X-ray fluorescence spectrometry (XRF, Zetium, PANalytical) was employed to identify the chemical composition of PRA.

The stability of the as-prepared catalysts was assessed by quantifying total iron ion contents using ICP-OES (AVIO 500, Perkin Elmer) to determine iron release from the composites. In the catalytic experiments, the concentration of TC in solution (C<sub>0</sub> = 80 mg/L) after the experiments was measured by UV-Vis spectrophotometry. The TC solution (C<sub>0</sub> = 80 mg/L) treated with MPRA1-2-800 was also analyzed by liquid chromatography-mass spectrometry (ESI<sup>-</sup> mode, Agilent Technologies). A TOC analyzer (multi N/C 3100, Analytik Jena) was used to quantify the degree of mineralization by measuring the total organic carbon (TOC) removal.

### 2.4. Experimental procedure for TC degradation

**TC degradation by Fenton reaction:** Using 250 mL conical flasks, 0.2 g of MPRA was mixed with 200 mL of 80 mg/L TC solution. The flasks were placed in a thermostat water bath (Model TOL09-FTSH- 01, SCIFINTECH) at a temperature of 28 ± 2 °C, and shaken at 200 rpm for 1 h while maintaining the pH of the mixture at 3.7. After 1 h, the TC solution was sampled to measure concentration, and H<sub>2</sub>O<sub>2</sub> (1–10 mM) was added to initiate the reaction. The influence of solution pH on the degradation of TC was tested by altering pH with 0.1 M HCl or 0.1 M NaOH. These experiments were conducted in darkness. After specific time periods (0–4 h), a magnet was used to separate the MPRA from solution, and TC

concentration was determined. TC concentration before and after the initiation of the Fenton reaction was measured by UV-Vis spectrophotometry (UV 2600, Shimadzu) via a calibrated approach at  $\lambda = 357$  nm. Degradation efficiency was calculated from formula (1):

$$\%Efficiency = \frac{(C_0 - C_t)}{C_0} \times 100 \quad (1)$$

where  $C_t$  denotes the concentration of TC at specific time periods, measured in mg/L.

**Catalyst regeneration:** A 0.2 g sample was combined with 200 mL of an 80 mg/L TC solution. The mixture was then shaken in a thermostat water bath for 4 h at  $28 \pm 2$  °C. The pH value was carefully controlled at 3.7. Subsequently, 5 mM of  $H_2O_2$  was added to the mixture. An external magnet was used to isolate the catalyst. The collected catalyst was then heated in air at 300 °C to be reactivated. A further four experimental runs were then carried out using the same sample of magnetic catalyst.

### 3. Results and discussion

#### 3.1. Optimization of the preparation conditions

The pyrolysis temperature was preliminarily optimized in the range of 600–800 °C under a  $N_2$  atmosphere. The preliminary results showed that the samples pyrolyzed at 600 and 700 °C (MPRA1-2-600 and MPRA1-2-700) displayed very low magnetization values (Fig. 1 and Table S1) and cannot be attracted by an external magnet. Only samples pyrolyzed at 800 °C were attracted to a magnet (Fig. S1A-C). In comparison to the samples calcined at 600 and 700 °C, the one calcined at 800 °C (MPRA1-2-800) showed stronger peak intensities at  $35.6^\circ$  (311) and  $62.5^\circ$  (440) corresponding to magnetite ( $Fe_3O_4$ , JCPDS No. 01-076-5948). Specifically, only the diffraction pattern of MPRA1-2-800 revealed a distinct peak of magnetite at  $30.33^\circ$  (220) as shown in Fig. S1D. These findings indicate a greater extent of magnetite formation at 800 °C than at 600 °C and 700 °C. Therefore, the pyrolysis temperature of 800 °C was suitable and was used for the synthesis of further samples.

The effect of the iron scrap-PRA weight ratio on the physical appearance of the catalyst was investigated. Images of MPRA1-1-800, MPRA1-2-800, MPRA1-4-800, and Scrap-800 are shown in Fig. S2. Their yields are listed in Table S1. PRA was dark grey in color while iron

scrap powder was red. The magnetic properties of MPRA1-1-800, MPRA1-2-800, MPRA1-4-800, and Scrap-800 were also measured by VSM. All four samples produced hysteresis loops within the  $\pm 10$  kOe range at a temperature of 300 K (Fig. 1), indicating their ferromagnetic nature. It was noted that the saturation magnetization values ( $M_s$ ) of the sample series were well correlated to the weight of iron scrap in the samples. The magnetization of MPRA1-4-800 was only 0.31 emu/g. The sample was barely attracted to the magnet due to the relatively low amount of iron scrap used in the preparation process. All the other samples were attracted to the magnet. Scrap-800 was prepared using only iron scrap but the magnetization of Scrap-800 was lower than MPRA1-1-800, indicating that the use of PRA as a catalyst support prevented the aggregation of magnetic iron oxide particles and maintained magnetic properties (Castillo et al., 2021; Chen et al., 2022; Thangaraj et al., 2019). Thus, the inclusion of PRA improved the magnetic properties of the composite. After pyrolysis, the MPRA samples were darker in color. The degree of darkening was proportional to the ratio of iron scrap in the sample and was attributed to the presence of iron oxide, probably magnetite, in the materials (Fig. S2).

#### 3.2. Characterization of MPRA catalysts

The FESEM-EDX results for all samples in Fig. S3 show that the particles of MPRA were rougher than the particles of PRA. The increased surface roughness of MPRA was due to the iron oxide particles precipitated on the PRA surface. EDX mapping of all MPRA samples revealed a uniform distribution of iron particles, along with calcium, oxygen, and silicon elements. The average iron contents of the MPRA samples were 6.6 wt% for MPRA-1-4-800, 14.7 wt% for MPRA-1-2-800, and 43.3 wt% for MPRA-1-1-800 (Table S2). These results exhibited a strong correlation with their respective magnetization values.

The presence of iron oxide particles was also confirmed by XRD analysis (Fig. 2). The patterns of magnetite ( $Fe_3O_4$ , JCPDS No. 01-076-5948) and hematite ( $Fe_2O_3$ , JCPDS No. 01-079-1741) were observed, indicating that mixed phases of iron were formed during pyrolysis due to the uncontrolled mole ratio between  $Fe^{2+}$  and  $Fe^{3+}$  in the iron scrap solution (Yi et al., 2019). Both forms of iron oxide were also detected in the Scrap-800 sample. Additionally, silica ( $SiO_2$ , JCPDS No. 03-065-0466) from PRA was detected in all MPRA samples. Notably, in agreement with the EDX results, calcite ( $CaCO_3$ , JCPDS No. 01-078-4614) was detected in the PRA sample, but the maximum intensity of the calcite peaks was very low compared to the maximum intensity of the silica peak at  $26.64^\circ 2\theta$ . Additionally, sylvite (KCl, JCPDS No. 01-075-0296) was also detected in all MPRA samples. XRF spectrometry was used to confirm the presence of calcite and silica in the PRA sample. The XRF analysis revealed that the composition of PRA included 48.48 %wt  $SiO_2$ , 22.03 %wt CaO, 6.96 %wt  $K_2O$ , and 5.81 %wt  $Al_2O_3$ , along with 3.48 %wt CHNO. This analysis indicated that silica and calcite were the main constituents of PRA.

The functional groups on the surface of the catalysts were examined using FTIR spectroscopy. Detailed band assignments were listed in Table S3. The absorption bands around  $3435\text{ cm}^{-1}$  were attributed to the stretching vibrations of O-H of adsorbed water and silanol groups (Si-OH). The absorption bands in the range of  $1700\text{--}1400\text{ cm}^{-1}$  indicated stretching vibrations of C-O bonds of carbonate groups and C=C bonds, suggesting the presence of  $CaCO_3$  and carbon materials in the samples. Additionally, the peak at  $\sim 1076\text{ cm}^{-1}$  was attributed to the stretching vibrations of Si-O-Si bonds, indicating the presence of silica in PRA (Fig. S4). Therefore, PRA contained silica,  $CaCO_3$ , and carbon materials. After the preparation process, a significant amount of  $CaCO_3$  had been eliminated by HCl, and a new absorption band was present in the spectra of MPRA samples at  $563\text{ cm}^{-1}$ , which was associated with the stretching vibrations of Fe-O bonds from iron oxides.

Fig. 3 presents the wide-scan XPS spectrum of MPRA1-2-800 and the high-resolution C 1s, O 1s, Si 2p, and Fe 2p spectra of the same sample. The XPS survey scan confirmed the presence of C, O, Si, and Fe in

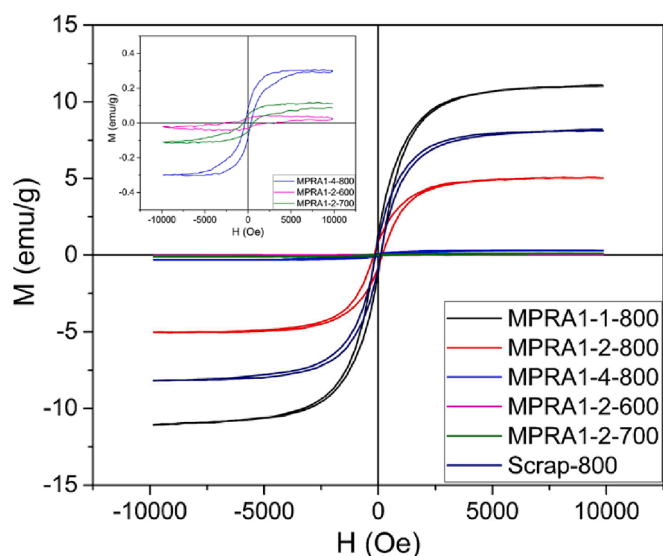


Fig. 1. The magnetic hysteresis loops for MPRA1-1-800, MPRA1-2-800, MPRA1-4-800, MPRA1-2-600, MPRA1-2-700 and Scrap-800 samples. The inset displays a zoomed-in view of the magnetic hysteresis loops for the MPRA1-4-800, MPRA1-2-600, and MPRA1-2-700 samples.

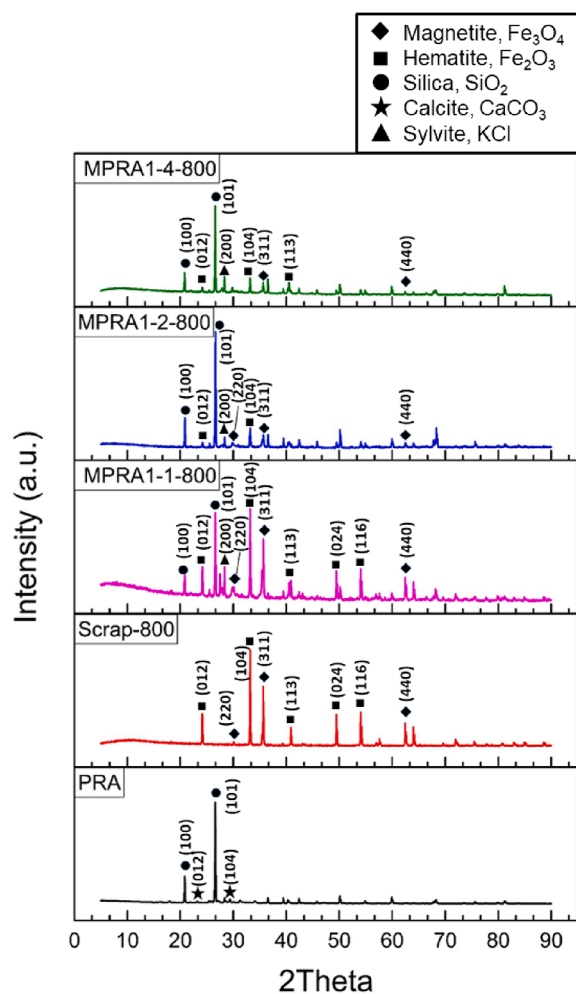
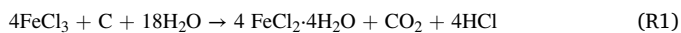


Fig. 2. XRD patterns of MPRA1-1-800, MPRA1-2-800, MPRA1-4-800, Scrap-800, and PRA samples.

MPRA1-2-800, and the high-resolution C 1 s and O 1 s spectra showed the presence of oxygenated functional groups that included carboxylic, hydroxyl, and ether groups. These groups were responsible for the hydrophilic properties of the catalyst. The peak at around 530 eV binding energy was attributed to magnetite ( $\text{Fe}_3\text{O}_4$ ) (Zhu et al., 2016). This finding was consistent with the presence of the band associated with Fe-O bonding at around  $559\text{ cm}^{-1}$  in the FTIR spectra and the XRD data. Moreover,  $\text{CaCO}_3$  and  $\text{SiO}_2$  were found in all MPRA samples. These were the inorganic compounds left from the pyrolysis process. The Fe 2p spectrum confirmed the presence of Fe(II) and Fe(III) in MPRA1-2-800. More specifically, the peaks at 710.66 and 723.76 eV verified the presence of Fe(II) in magnetite form. Table S4 contains the comprehensive peak assignments for the deconvoluted XPS peaks derived from the XPS spectra, along with their corresponding binding energies. The high-resolution Fe 2p spectrum confirmed the presence of both  $\text{Fe}^{2+}$  and  $\text{Fe}^{3+}$  (36.5:63.5 %at) from the magnetite structure in the materials. These findings corroborated the presence of magnetite particles on the surface of PRA.

During the synthesis of MPRA by pyrolysis, the residual carbon in PRA reduced  $\text{Fe}^{3+}$  to  $\text{Fe}^{2+}$  and then both  $\text{Fe}^{2+}$  and  $\text{Fe}^{3+}$  formed magnetite and hematite. The process is described in reactions R(1)–R(3) (Liu et al., 2020; Wang et al., 2021).



Subsequently, iron oxide particles were precipitated and deposited onto the surface of PRA, leading to the acquisition of magnetic properties.

### 3.3. Effect of reaction conditions on the catalytic activity of MPRA

This section focuses on examining the MPRA composite as a heterogeneous Fenton catalyst, specifically investigating the catalytic degradation of TC. First, an 80 ppm TC solution at pH 3.7 was shaken in darkness for 1 h on MPRA at a catalyst concentration of 1 g/L. The reaction was then initiated by introducing 5 mM of  $\text{H}_2\text{O}_2$ . MPRA1-2-800 showed the highest removal efficiency at  $\sim 95\%$  (Fig. 4A). MPRA1-1-800 removed  $\sim 66\%$  of TC after a 4-hour reaction time, even though the iron content in MPRA1-1-800 was higher. The Scrap-800 control removed only  $\sim 40\%$  of TC. In the absence of the catalyst (only 5 mM of  $\text{H}_2\text{O}_2$  with TC), only 5.66% of TC was removed. This finding shows that the presence of PRA as a catalyst support considerably enhanced removal efficiency. The degree of Fe leaching was 1.65, 2.74, and 4.45 mg/L for MPRA1-1-800, MPRA1-2-800, and Scrap-800, respectively. This result indicated the lower stability of Scrap-800 due to the lack of support material. Although MPRA1-1-800 had a higher magnetization value with better stability than MPRA1-2-800, MPRA1-2-800 showed a significantly higher efficiency toward TC removal. BET surface area analysis (Table S5) revealed that the BET surface area of MPRA1-2-800 was bigger, which was a beneficial characteristic because it allowed TC molecules greater accessibility to active sites. As a result, MPRA1-2-800 was selected as the most promising Fenton catalyst for the catalytic degradation of TC. This choice was based on its capacity to remove TC, its satisfactory level of iron leaching, and its strong magnetic characteristics.

The pH level is a crucial determinant in the Fenton-like reaction (Lai et al., 2019; Wang et al., 2016). The effect of initial solution pH on the catalytic degradation of TC using MPRA1-2-800 is shown in Fig. 4B. At a pH solution of 3.7, up to 90% of TC was removed within 15 min, and 95.61% in 4 h. This result is consistent with the fact that an acidic solution is often the suitable condition for most Fenton-like catalysts (Subramanian et al., 2016). Moreover, TC degradation remained nearly the same when the pH was increased from 3.7 to 9.0, indicating that this Fenton system can be applied in a wide pH range, therefore overcoming the costly requirement of classical Fenton systems for an acidic condition that also results in secondary pollution of iron sludge. However, the effectiveness of the reaction notably decreased as the pH of the solution approached 12 due to a reduction in the reactivity of the radicals and the precipitation of iron. (Subramanian et al., 2016). Hence, the pH of 3.7 was selected as the optimal pH for subsequent experiments. The results were analyzed using the BMG kinetic model to assess the kinetics of TC catalytic degradation (Behnajady et al., 2007; Sidney Santana et al., 2019) as in Equation (2),

$$\frac{t}{\left(1 - \frac{C}{C_0}\right)} = m + bt \quad (2)$$

where C is the TC concentration at time t (min) and  $C_0$  is the initial concentration of TC at time t = 0. Additionally, b and m are two characteristic constants associated with the reaction kinetics and oxidation capacities. The kinetics of TC degradation on MPRA1-2-800 fitted well with the BMG kinetic model with an  $R^2$  close to 1 (Fig. S5). The reciprocal of the b value is the theoretical maximum TC fraction that can be removed, which is equal to the maximum oxidation capacity at the end of the reaction. Meanwhile,  $1/m$  is the initial rate of TC removal. In this work, the value of  $1/b$  was 0.944, which is close to 1 (maximum capacity) and the value of  $1/m$  was 1.491, which is very high. This model suggests that the oxidation of TC by Fenton-like processes, utilizing iron as a catalyst, typically proceeds in two stages: a rapid initial stage and a slower secondary stage. The initial rapidity of the process was ascribed

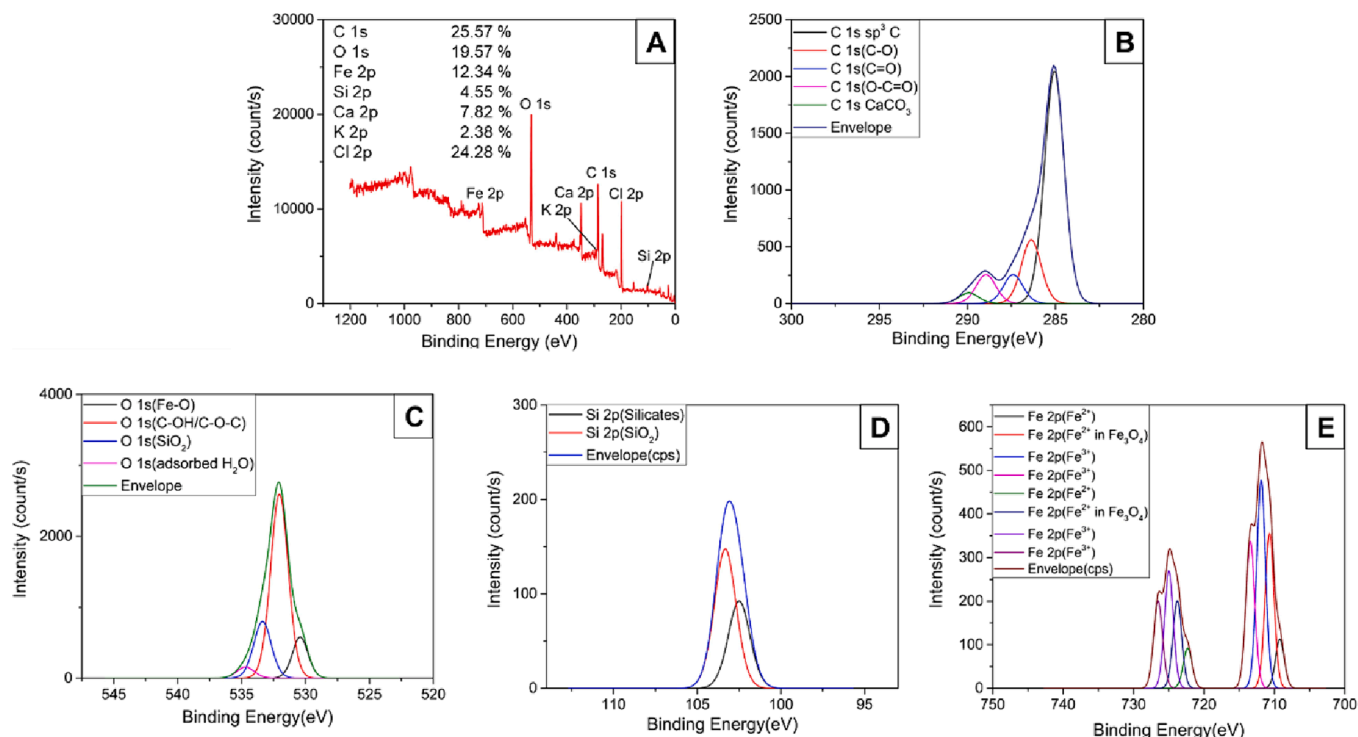


Fig. 3. (A) The wide-scan XPS and (B-E) high-resolution C 1s, O 1s, Si 2p, and Fe 2p spectra of MPRA1-2-800.

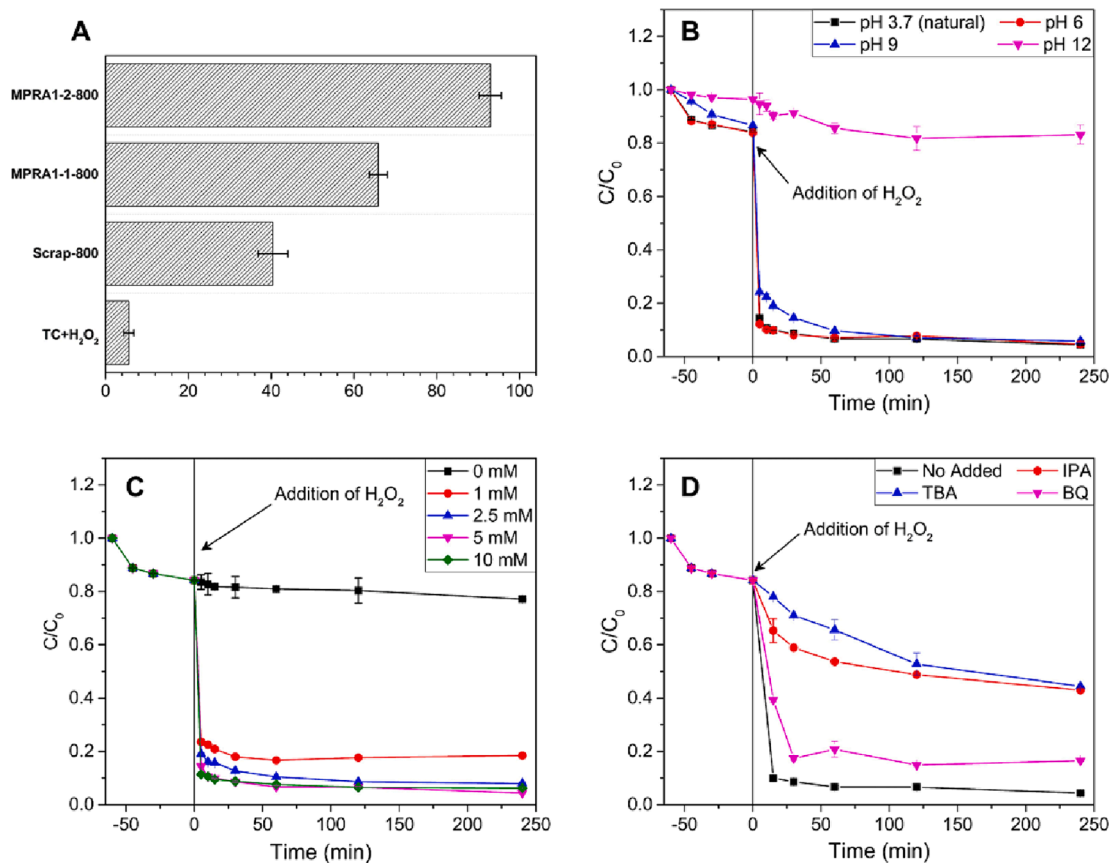


Fig. 4. (A) Results from the preliminary test of the catalytic heterogeneous Fenton-like reaction and the catalytic degradation of TC; (B) effect of initial pH; (C) effect of H<sub>2</sub>O<sub>2</sub> concentration; and (D) scavenger test. (Conditions: TC initial concentration (C<sub>0</sub>) is 80 mg/L, pH is 3.7 (natural), 5 mM H<sub>2</sub>O<sub>2</sub>, catalyst dosage of 1 g/L, and temperature at 28 ± 2 °C).

to the reaction between dissolved iron ions and  $H_2O_2$ , while the subsequent slower rate was caused by the accumulation of  $Fe^{3+}$  and the limited regeneration of  $Fe^{2+}$  by  $H_2O_2$ . This finding was consistent with the rate constant of the reaction between  $Fe^{2+}$  and  $H_2O_2$ , which is generally higher than that of the reaction between  $Fe^{3+}$  and  $H_2O_2$  in homogeneous reactions. When these two competing processes consume  $H_2O_2$ , the concentration of  $H_2O_2$  in the solution is gradually reduced to a low level, the retardation stage begins, and the small amount of oxidant in the solution becomes a limiting factor.

A succession of trials was carried out using  $H_2O_2$  concentrations of 0, 1, 2.5, 5, and 10 mM to investigate the influence of different quantities on the catalytic degradation of TC (Fig. 4C). An absence of  $H_2O_2$  in the adsorption experiment restricted the elimination of TC to 22.8 %, owing to the shortage of adsorption sites and the low BET surface area. Nonetheless, as the concentration of  $H_2O_2$  increased, the effectiveness of MPRA1-2-800 increased. After 4 h, 5 mM  $H_2O_2$  had removed 95.61 % of TC. However, the removal of TC in 10 mM  $H_2O_2$  was relatively unchanged because the surplus  $H_2O_2$  competed with TC for  $\cdot OH$  in the following reactions (Lai et al., 2019):



Thus, the optimal concentration of  $H_2O_2$  was 5 mM.

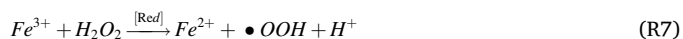
To identify the free radicals involved in the Fenton-like reaction, free radical scavengers were incorporated into the reaction solution. Hydroxyl radicals ( $\cdot OH$ ) were trapped with 0.3 M *tert*-butyl alcohol (TBA), and superoxide radicals ( $\cdot O_2^-$ ) were trapped with 20 mM *p*-benzoquinone (BQ) (Hou et al., 2016; Ma et al., 2018). TBA significantly hindered TC degradation but 20 mM BQ had only a small effect on TC degradation (Fig. 4D). It was concluded that  $\cdot OH$  served as the main reactive oxygen species in this heterogeneous Fenton-like system and to confirm that the Fenton-like reaction was induced by  $\cdot OH$  radicals, 0.3 M isopropanol (IPA) was added to the reaction to differentiate between adsorbed and unbound hydroxyl radicals. Generally, TBA can suppress both free hydroxyl radicals in solution ( $\cdot OH_{free}$ ) and hydroxyl radicals adsorbed onto the catalyst surface ( $\cdot OH_{ads}$ ), whereas IPA can only suppress  $\cdot OH_{free}$ . The degradation of TC was substantially inhibited by the addition of IPA, and removal efficiency was comparable to that achieved in the presence of TBA. These results suggested that  $\cdot OH_{free}$  contributed to the degradation of TC, while  $\cdot OH_{ads}$  and  $\cdot O_2^-$  had very minor impacts.

The total organic carbon (TOC) content of the TC solution was determined both before and after catalytic degradation. This evaluation provided additional evidence that the primary mechanism for TC removal was catalytic degradation and not adsorption. The removal of TOC was found to be 90.81 %, indicating the mineralization of TC during the Fenton-like reaction. Moreover, a solution of 80 ppm TC was analyzed by LC-MS before and after degradation on MPRA1-2-800. The loss of the  $m/z$  peak at 443.16 after degradation (Fig. S6) suggested that the intermediates quickly underwent oxidation to inorganic compounds.

The LC-MS analysis was used to explore the mechanism of degradation. A possible degradation pathway was proposed in Fig. S7. The peak at  $m/z$  325.18 has been associated previously with TC degradation and confirms the presence of the intermediate P4 ( $C_{19}H_{18}O_5$ ) (Huang et al., 2020), suggesting that fresh TC molecules ( $m/z = 443$ ) first degraded into P1 ( $m/z = 461$ ) via hydroxylation at position 14, and then P1 was further decomposed into P2 ( $m/z = 429$ ) by losing the methyl in the amino group. After that, the amide of P2 was attacked by reactive radicals, which resulted in the production of P3 ( $m/z = 371$ ). P3 continuously converted to smaller structures of P4 ( $m/z = 325$ ) through dehydroxylation and the oxidation of the  $-NHCH_3$  group at positions 1 and 2, respectively. Subsequently, the double bond at position 1 was attacked, leading to a ring cleavage reaction, and an aldehyde group was formed at position 17, producing P5 ( $m/z = 272$ ) which was further decomposed to P6 ( $m/z = 179$ ). Finally, the molecules P6 were further oxidized into smaller products via subsequent reactions such as ring

cleavage and mineralization into inorganic compounds such as  $CO_2$  and  $H_2O$ .

The mechanism of the Fenton-like reaction on the MPRA1-2-800 catalyst is proposed as shown in R6-R10 (Ameta et al., 2018; Gan et al., 2020; Tang & Wang, 2018). Initially, the iron oxide on the surface of MPRA1-2-800 dissolves rapidly in the acidic condition. Subsequently, iron ions ( $Fe^{2+}/Fe^{3+}$ ) engage in a reaction with  $H_2O_2$ , resulting in the formation of hydroxyl radicals ( $\cdot OH$ ), perhydroxyl radicals ( $\cdot OOH$ ), and superoxide radicals ( $\cdot O_2^-$ ), as shown in R6-R8. To maintain the catalytic cycle,  $Fe^{2+}$  is regenerated through the reduction of  $Fe^{3+}$ , as described by R9-R10.



The dissolution of the iron ions into the solution, due to the acidic condition, was considered inevitable, leading to the leaching of Fe into the solution. However, the Fe concentration determined by ICP-OES was 2.74 mg/L, which does not exceed the maximum concentration permitted in industrial areas of Thailand (<10 mg/L).

### 3.4. The regeneration of MPRA1-2-800

Catalyst regeneration was studied because it is a crucial criterion of practicality. The reusability of MPRA1-2-800 was tested by degrading 200 mL of 80 mg/L TC solution for 4 h, at pH 3.7 with the addition of 5 mM of  $H_2O_2$ . The used sample was then regenerated by heat treatment at 300 °C for 1 h in air to expose more iron oxide as active sites. The reactivated catalyst was then used again to degrade TC. As shown in Fig. 5A, the degradation of TC on the fresh catalyst was 95.61 %. After four cycles of use, degradation efficiency was 67.40 % which is an acceptable level. The degree of Fe leaching was only high during the first use and, afterwards was less than 0.5 mg/L until the fourth cycle (Fig. 5B). Despite the Fe leaching, the magnetic properties of the catalyst were maintained, indicating the good stability of the catalyst. Moreover, the high-resolution XPS spectra of the used catalyst in Fig. S8 showed that the surface chemistry of used MPRA1-2-800 after four cycles was similar to the surface chemistry of fresh catalyst (Fig. 3). Interestingly, the Fe(II)-Fe(III) ratio from Fe 2p in Table S4 was changed from 1:2 to 1:1, indicating that circulation of Fe(II) and Fe(III) occurred during the Fenton-like reaction. This behavior could enhance degradation efficiency because the rate constant of the Fenton reaction is higher when  $Fe^{2+}$  is involved (R6) than  $Fe^{3+}$  (R7) (Wang et al., 2021). Furthermore, the used MPRA1-2-800 was characterized by VSM analysis (Fig. 5C). The saturation magnetization of used MPRA1-2-800 was lower but the catalyst was still attracted to the magnet. The decrease in magnetic strength may be attributed to a combination of factors, including the leaching of iron, and the air oxidation during the air-calcination regeneration process. Following four cycles of catalyst use, the %Fe content from the EDX analysis decreased slightly, from 14.70 to 13.50 % (Table S2). Fe leaching should thus not be a primary cause of the loss of magnetic strength. The primary cause should be the air-calcination process, since oxygen gas in the air may gradually oxidize the magnetic phase to the non-magnetic phase.

### 3.5. Comparative analyses

To assess the performance of MPRA1-2-800 as a Fenton-like catalyst

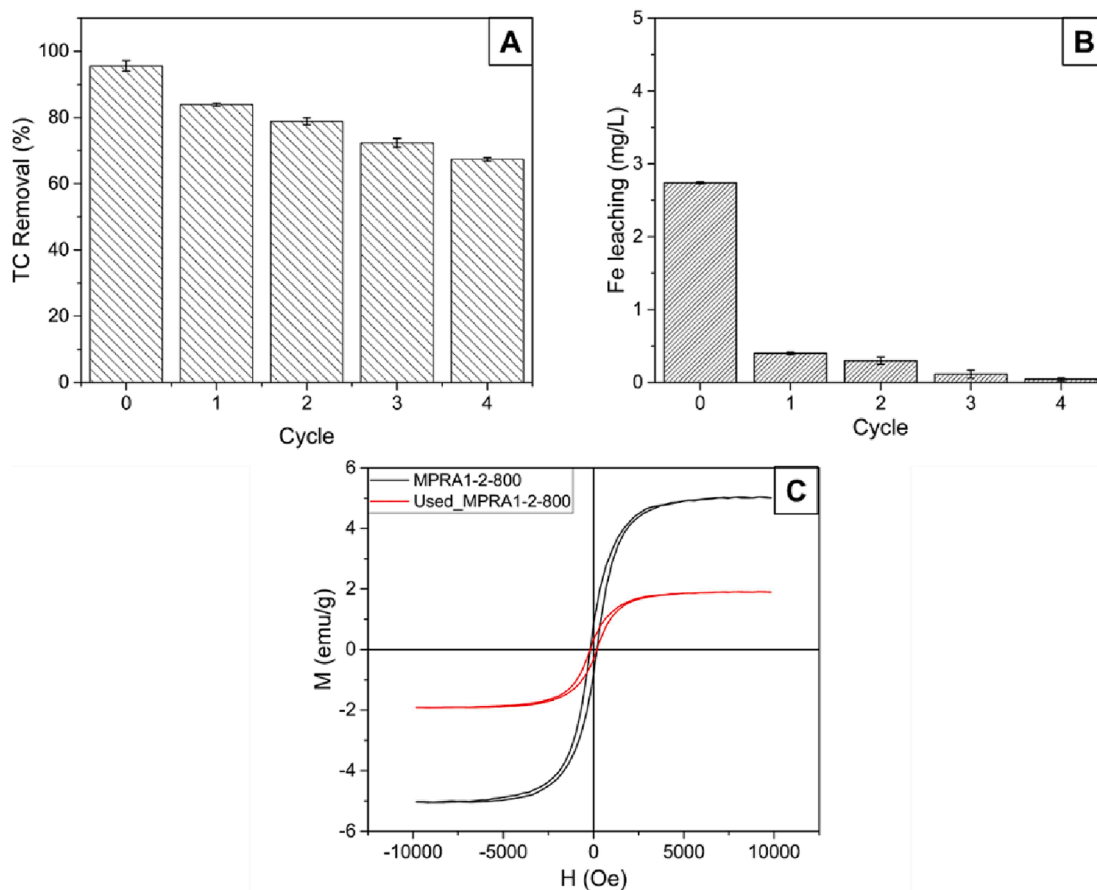


**Fig. 5.** The regeneration experiments determined (A) the degradation of TC on MPRA1-2-800 over four cycles; (B) the amount of iron leaching after each cycle obtained from ICP-OES analysis; and (C) the magnetic hysteresis loop of the fresh MPRA1-2-800 sample and the used MPRA1-2-800 sample. (Conditions: TC initial concentration ( $C_0$ ) of 80 mg/L, pH of 3.7 (natural), 5 mM  $H_2O_2$ , catalyst dosage of 1 g/L, and temperature at  $28 \pm 2$  °C).

for TC degradation, a comparison was made with previous studies (Table S6). In terms of efficiency, the MPRA1-2-800 removed 90 % of TC within 15 min and up to 94.35 % in 4 h. Most previous studies used quite low concentrations or a small volume of TC solution, leading to a high removal percentage. This is reflected by the actual amount of removed TC in mg which confirms the high performance of the proposed Fenton-like catalyst compared to other catalysts. Although some studies used hybrid systems between Fenton and other techniques such as UV-Fenton degradation, ultrasound-assisted Fenton-like degradation, and photo-Fenton degradation, their actual removal values were low compared to this work. Also, the  $H_2O_2$  concentration is a key factor that affects operating costs. The  $H_2O_2$  concentration used in this work was quite low compared to previous reports, leading to better cost effectiveness for a real operation. Additionally, the high TOC removal in the present work indicates the effective degradation of TC by mineralization and oxidation. Secondary contamination from intermediates is therefore minimal, which cannot be said for processes in some other works that reported low TOC removal values. Furthermore, the Fenton-like catalyst in this work was prepared by a simple pyrolysis method using only para-rubber wood ash and iron scrap as precursors, which are waste industrial materials. On the contrary, previous studies described complicated procedures and used harmful chemicals, in particular some highly toxic heavy metals were utilized to accelerate Fe(II)/Fe(III) circulation, which must lead to secondary contamination. Therefore, MPRA1-2-800 is a promising Fenton-like catalyst for water remediation.

#### 4. Conclusion

A magnetic catalyst was synthesized from para-rubber wood ash and

iron scrap by pyrolysis. The catalyst was used for the degradation of tetracycline in a Fenton system. Extensive characterizations confirmed the uniform distribution of iron oxide species on the para-rubber wood ash support material. The most effective catalyst removed more than 90 % of tetracycline within 15 min under optimal conditions (1 g/L catalyst dose, 5 mM  $H_2O_2$ , pH 3.7, and 80 mg/L tetracycline solution), while demonstrating excellent magnetic properties and good stability. The removal percentage exceeded those previously reported, highlighting the potential of the proposed catalyst for the Fenton-like degradation of antibiotics in wastewater. Scavenging experiments indicated that hydroxyl radicals were the major reactive species in the catalytic Fenton system. LC-MS analysis identified reaction intermediates, enabling the proposal of a possible pathway of tetracycline degradation. Additionally, the catalyst could be recycled with minimal Fe leaching, retaining stability over four cycles. Further research might prioritize the expansion of synthesis on a larger scale, investigating its effectiveness against different contaminants, and evaluating its real-world performance to promote sustainable wastewater treatment.

#### CRediT authorship contribution statement

**Natthanan Rattanachueskul:** Formal analysis, Investigation, Methodology, Validation, Writing – original draft, Writing – review & editing. **Parichart Onsri:** Formal analysis, Investigation. **Waralee Watcharin:** Investigation. **Arthit Makarasen:** Investigation. **Supanna Techasakul:** Supervision, Visualization, Writing – review & editing. **Decha Dechtrirat:** Conceptualization, Funding acquisition, Methodology, Project administration, Validation, Writing – original draft, Writing – review & editing. **Laemthong Chuenchom:** Conceptualization,

Formal analysis, Funding acquisition, Methodology, Validation, Writing – original draft, Writing – review & editing.

### Declaration of competing interest

The authors declare that they have no known competing financial interests or personal relationships that could have appeared to influence the work reported in this paper.

### Acknowledgements

The authors would like to thank the Kasetsart University Research and Development Institute (grant No. FF(KU)27.67) for financial support. N. Rattanachueskul also thanks the Graduate School, Prince of Songkla University, for PSU-PhD. scholarship (Contract No. PSU\_PHD2562-003) and financial support, and the Division of Physical Science, Faculty of Science, Prince of Songkla University, Thailand, for support with facilities. L. Chuenchom acknowledges partial support from the Center of Excellence for Innovation in Chemistry (PERCH-CIC), Ministry of Higher Education, Science, Research, and Innovation, Thailand. The authors are also indebted to Thomas Duncan Coyne and Dr. Titilope John Jayeoye for English proof-reading and editing.

### Appendix A. Supplementary material

Supplementary data to this article can be found online at <https://doi.org/10.1016/j.arabjc.2024.105791>.

### References

- Abdul Mutalib, A.A., Ibrahim, M.L., Matmin, J., Kassim, M.F., Mastuli, M.S., Taufiq-Yap, Y.H., Shohaimi, N.A.M., Islam, A., Tan, Y.H., Kaus, N.H.M., 2020. SiO<sub>2</sub>-rich sugar cane bagasse ash catalyst for transesterification of palm oil. *Bioenergy Res.* 13, 986–997. <https://doi.org/10.1007/s12155-020-10119-6>.
- Agú, U.A., Mendieta, S.N., Gerbaldo, M.V., Crivello, M.E., Casuscelli, S.G., 2020. Highly active heterogeneous fenton-like system based on cobalt ferrite. *Ind. Eng. Chem.* 59 (4), 1702–1711. <https://doi.org/10.1021/acs.iecr.9b04042>.
- Ameta, R., K. Chohadia, A., Jain, A., Punjabi, P.B. 2018. Chapter 3 - Fenton and photo-Fenton processes. in: *Adv. Oxid. Processes Wastewater Treat.* (Eds.) S.C. Ameta, R. Ameta, Academic Press, pp. 49–87.
- Babar, S., Gavade, N., Shinde, H., Mahajan, P., Lee, K.H., Mane, N., Deshmukh, A., Garadkar, K., Bhuse, V., 2018. Evolution of waste iron rust into magnetically separable g-C<sub>3</sub>N<sub>4</sub>-Fe<sub>2</sub>O<sub>3</sub> photocatalyst: an efficient and economical waste management approach. *ACS Appl. Nano Mater.* 1 (9), 4682–4694. <https://doi.org/10.1021/acsnm.8b00936>.
- Behnajady, M.A., Modirshahla, N., Ghanbary, F., 2007. A kinetic model for the decolorization of C.I. acid yellow 23 by Fenton process. *J. Hazard. Mater.* 148 (1), 98–102. <https://doi.org/10.1016/j.jhazmat.2007.02.003>.
- Castillo, J., Vargas, V., Macero, D., Le Beulze, A., Ruiz, W., Bouyssiére, B., 2021. One-step synthesis of SiO<sub>2</sub>-α-Fe<sub>2</sub>O<sub>3</sub>/Fe<sub>3</sub>O<sub>4</sub> composite nanoparticles with magnetic properties from rice husks. *Phys. B: Condens. Matter.* 605, 412799 <https://doi.org/10.1016/j.physb.2020.412799>.
- Chandane, P., Ladke, J., Jori, C., Deshmukh, S., Zinjardé, S., Chakankar, M., Hocheng, H., Jadhav, U., 2019. Synthesis of magnetic Fe<sub>3</sub>O<sub>4</sub> nanoparticles from scrap iron and use of their peroxidase like activity for phenol detection. *J. Environ. Chem. Eng.* 7 (3), 103083 <https://doi.org/10.1016/j.jece.2019.103083>.
- Chen, L., Costa, E., Kileti, P., Tannenbaum, R., Lindberg, J., Mahajan, D., 2022. Sonochemical synthesis of silica-supported iron oxide nanostructures and their application as catalysts in Fischer-Tropsch synthesis. *Micro* 2, 632–648.
- Chen, W.-H., Huang, J.-R., Lin, C.-H., Huang, C.-P., 2020. Catalytic degradation of chlorpheniramine over GO-Fe<sub>3</sub>O<sub>4</sub> in the presence of H<sub>2</sub>O<sub>2</sub> in water: The synergistic effect of adsorption. *Sci. Total Environ.* 736, 139468 <https://doi.org/10.1016/j.scitotenv.2020.139468>.
- Chen, J.-Q., Zhou, G.-N., Ding, R.-R., Li, Q., Zhao, H.-Q., Mu, Y., 2023. Ferrous ion enhanced Fenton-like degradation of emerging contaminants by sulfidated nanosized zero-valent iron with pH insensitivity. *J. Hazard. Mater.* 459, 132229 <https://doi.org/10.1016/j.jhazmat.2023.132229>.
- Choi, K.-J., Kim, S.-G., Kim, S.-H., 2008. Removal of antibiotics by coagulation and granular activated carbon filtration. *J. Hazard. Mater.* 151 (1), 38–43. <https://doi.org/10.1016/j.jhazmat.2007.05.059>.
- Deganello, F., Joshi, M., Liotta, L.F., La Parola, V., Marci, G., Pantaleo, G., 2019. Sustainable recycling of insoluble rust waste for the synthesis of iron-containing perovskite-type catalysts. *ACS Omega* 4 (4), 6994–7004. <https://doi.org/10.1021/acsomega.8b03522>.
- Do, Q.C., Kim, D.-G., Ko, S.-O., 2018. Catalytic activity enhancement of a Fe<sub>3</sub>O<sub>4</sub>@SiO<sub>2</sub> yolk-shell structure for oxidative degradation of acetaminophen by decoration with copper. *J. Clean. Prod.* 172, 1243–1253. <https://doi.org/10.1016/j.jclepro.2017.10.246>.
- Dutta, J., Mala, A.A., 2020. Removal of antibiotic from the water environment by the adsorption technologies: A review. *Water Sci. Technol.* 82 (3), 401–426. <https://doi.org/10.2166/wst.2020.335>.
- Farhadian, N., Liu, S., Asadi, A., Shahlaei, M., Moradi, S., 2021. Enhanced heterogeneous Fenton oxidation of organic pollutant via Fe-containing mesoporous silica composites: A review. *J. Mol. Liq.* 321, 114896 <https://doi.org/10.1016/j.molliq.2020.114896>.
- Fatimah, I., Amaliah, S.N., Andrian, M.F., Handayani, T.P., Nurillahi, R., Prakoso, N.I., Wicaksono, W.P., Chuenchom, L., 2019. Iron oxide nanoparticles supported on biogenic silica derived from bamboo leaf ash for rhodamine B photodegradation. *Sustain. Chem. Pharm.* 13, 100149 <https://doi.org/10.1016/j.scp.2019.100149>.
- Fatimah, I., Yanti, I., Wijayanti, H.K., Ramanda, G.D., Sagadevan, S., Tamyiz, M., Doong, R.-A., 2023. One-pot synthesis of Fe<sub>3</sub>O<sub>4</sub>/NiFe<sub>2</sub>O<sub>4</sub> nanocomposite from iron rust waste as reusable catalyst for methyl violet oxidation. *Case Stud. Chem. Environ. Eng.* 8, 100369 <https://doi.org/10.1016/j.csee.2023.100369>.
- Gan, Q., Hou, H., Liang, S., Qiu, J., Tao, S., Yang, L., Yu, W., Xiao, K., Liu, B., Hu, J., Wang, Y., Yang, J., 2020. Sludge-derived biochar with multivalent iron as an efficient Fenton catalyst for degradation of 4-chlorophenol. *Sci. Total Environ.* 725, 138299 <https://doi.org/10.1016/j.scitotenv.2020.138299>.
- Hasan, S., Hashim, M.A., Gupta, B.S., 2000. Adsorption of Ni(SO<sub>4</sub>) on Malaysian rubberwood ash. *Bioresour. Technol.* 72 (2), 153–158. [https://doi.org/10.1016/S0960-8524\(99\)00101-7](https://doi.org/10.1016/S0960-8524(99)00101-7).
- Hou, L., Wang, L., Royer, S., Zhang, H., 2016. Ultrasound-assisted heterogeneous Fenton-like degradation of tetracycline over a magnetite catalyst. *J. Hazard. Mater.* 302, 458–467. <https://doi.org/10.1016/j.jhazmat.2015.09.033>.
- Huang, X., Zhu, N., Mao, F., Ding, Y., Zhang, S., Liu, H., Li, F., Wu, P., Dang, Z., Ke, Y., 2020. Enhanced heterogeneous photo-Fenton catalytic degradation of tetracycline over yCeO<sub>2</sub>/Fh composites: Performance, degradation pathways, Fe<sup>2+</sup> regeneration and mechanism. *Chem. Eng. J.* 392, 123636 <https://doi.org/10.1016/j.cej.2019.123636>.
- Jiang, W., Dionysiou, D.D., Kong, M., Liu, Z., Sui, Q., Lyu, S., 2020. Utilization of formic acid in nanoscale zero valent iron-catalyzed Fenton system for carbon tetrachloride degradation. *Chem. Eng. J.* 380, 122537 <https://doi.org/10.1016/j.cej.2019.122537>.
- Khataee, A., Gholami, P., Vahid, B., 2017. Catalytic performance of hematite nanostructures prepared by N<sub>2</sub> glow discharge plasma in heterogeneous Fenton-like process for acid red 17 degradation. *J. Ind. Eng. Chem.* 50, 86–95. <https://doi.org/10.1016/j.jiec.2017.01.035>.
- Koch, G.H., Brongers, M.P.H., Thompson, N.G., Virmani, Y.P., Payer, J.H. 2002. Corrosion Costs and Preventive Strategies in the United States: Report by CC Technologies Laboratories, Inc. to Federal Highway Administration (FHWA); National Technical Information Service: Alexandria, VA.
- Krasucka, P., Pan, B., Sik Ok, Y., Mohan, D., Sarkar, B., Oleszczuk, P., 2021. Engineered biochar – A sustainable solution for the removal of antibiotics from water. *Chem. Eng. J.* 405, 126926 <https://doi.org/10.1016/j.cej.2020.126926>.
- Lai, C., Huang, F., Zeng, G., Huang, D., Qin, L., Cheng, M., Zhang, C., Li, B., Yi, H., Liu, S., Li, L., Chen, L., 2019. Fabrication of novel magnetic MnFe<sub>2</sub>O<sub>4</sub>/bio-char composite and heterogeneous photo-Fenton degradation of tetracycline in near neutral pH. *Chemosphere* 224, 910–921. <https://doi.org/10.1016/j.chemosphere.2019.02.193>.
- Le Blond, J.S., Woskie, S., Horwell, C.J., Williamson, B.J., 2017. Particulate matter produced during commercial sugarcane harvesting and processing: A respiratory health hazard? *Atmos. Environ.* 149, 34–46. <https://doi.org/10.1016/j.atmosenv.2016.11.012>.
- Li, X., Cui, K., Guo, Z., Yang, T., Cao, Y., Xiang, Y., Chen, H., Xi, M., 2020. Heterogeneous Fenton-like degradation of tetracyclines using porous magnetic chitosan microspheres as an efficient catalyst compared with two preparation methods. *Chem. Eng. J.* 379, 122324 <https://doi.org/10.1016/j.cej.2019.122324>.
- Li, H., Shi, B., Fu, X., Zhang, H., Yang, H., 2023. Preparation and application of red mud-based zero-valent iron heterogeneous Fenton catalyst: A new idea for red mud recycling. *J. Environ. Chem. Eng.* 11 (3), 109998 <https://doi.org/10.1016/j.jece.2023.109998>.
- Li, J., You, J., Wang, Z., Zhao, Y., Xu, J., Li, X., Zhang, H., 2022. Application of α-Fe<sub>2</sub>O<sub>3</sub>-based heterogeneous photo-Fenton catalyst in wastewater treatment: A review of recent advances. *J. Environ. Chem. Eng.* 10 (5), 108329 <https://doi.org/10.1016/j.jece.2022.108329>.
- Liu, Y., Huang, J., Xu, H., Zhang, Y., Hu, T., Chen, W., Hu, H., Wu, J., Li, Y., Jiang, G., 2020. A magnetic macro-porous biochar sphere as vehicle for the activation and removal of heavy metals from contaminated agricultural soil. *Chem. Eng. J.* 390, 124638 <https://doi.org/10.1016/j.cej.2020.124638>.
- Lu, Y., Qin, X., Wang, K., Chen, S., Quan, X., 2023. Accelerated Fe(II) regeneration on Fe-doped oxidized carbon nanotube enabling highly-efficient electro-Fenton process for pollutants removal. *Sep. Purif. Technol.* 320, 124196 <https://doi.org/10.1016/j.seppur.2023.124196>.
- Ma, X., Cheng, Y., Ge, Y., Wu, H., Li, Q., Gao, N., Deng, J., 2018. Ultrasound-enhanced nanosized zero-valent copper activation of hydrogen peroxide for the degradation of norfloxacin. *Ultrason. Sonochem.* 40, 763–772. <https://doi.org/10.1016/j.ultsonch.2017.08.025>.
- Ma, C., Jia, S., Yuan, P., He, Z., 2020. Catalytic ozonation of 2, 2'-methylenebis (4-methyl-6-tert-butylphenol) over nano-Fe<sub>3</sub>O<sub>4</sub>@cow dung ash composites: Optimization, toxicity, and degradation mechanisms. *Environ. Pollut.* 265, 114597 <https://doi.org/10.1016/j.envpol.2020.114597>.
- Madurwar, M., Mandavgane, S., Ralegaonkar, R., 2014. Use of sugarcane bagasse ash as brick material. *Curr. Sci.* 117, 1044–1051.

- Masae, M.S., L.; Kongsong, P.; Phoempon, P.; Rawangwong, S.; Sririkun, W. 2013. Application of rubber wood ash for removal nickel and copper from aqueous solution. *Environ. Nat. Resour. J.* 11(No.2), 17-27.
- Munoz, M., de Pedro, Z.M., Casas, J.A., Rodriguez, J.J., 2015. Preparation of magnetite-based catalysts and their application in heterogeneous Fenton oxidation – A review. *Appl. Catal. b: Environ.* 176–177, 249–265. <https://doi.org/10.1016/j.apcatb.2015.04.003>.
- Priya, S.S., Radha, K.V., 2017. A review on the adsorption studies of tetracycline onto various types of adsorbents. *Chem. Eng. Commun.* 204 (8), 821–839. <https://doi.org/10.1080/00986445.2015.1065820>.
- Priyadarshini, M., Ahmad, A., Ghangrekar, M.M., 2023. Efficient upcycling of iron scrap and waste polyethylene terephthalate plastic into Fe<sub>3</sub>O<sub>4</sub>@C incorporated MIL-53 (Fe) as a novel electro-Fenton catalyst for the degradation of salicylic acid. *Environ. Pollut.* 322, 121242 <https://doi.org/10.1016/j.envpol.2023.121242>.
- Purnomo, C.W., Respito, A., Sitanggang, E.P., Mulyono, P., 2018. Slow release fertilizer preparation from sugar cane industrial waste. *Environ. Technol. Inno.* 10, 275–280. <https://doi.org/10.1016/j.eti.2018.02.010>.
- Radoń, A., Łoński, S., Warski, T., Babilas, R., Tański, T., Dudziak, M., Łukowiec, D., 2019. Catalytic activity of non-spherical shaped magnetite nanoparticles in degradation of Sudan I, rhodamine B and methylene blue dyes. *Appl. Surf. Sci.* 487, 1018–1025. <https://doi.org/10.1016/j.apsusc.2019.05.091>.
- Rashmishree, K.N., Bhaskar, S., Shri Hari, S., Thalla, A.K. 2023. Green synthesis of laterite iron-based nanocatalysts using Psidium guajava and Macaranga peltata plant extract for its catalytic application in Fenton's oxidation of triclosan. *Clean Technol. Environ. Policy.* 10.1007/s10098-023-02507-1.
- Rodríguez-Díaz, J., García, J., Sánchez, L., Silva, M., Silva, V., Arteaga-Pérez, L., 2015. Comprehensive Characterization of sugarcane bagasse ssh for its use as an adsorbent. *Bioenergy Res.* 8, 1885–1895. <https://doi.org/10.1007/s12155-015-9646-6>.
- Saitoh, T., Shibata, K., Fujimori, K., Ohtani, Y., 2017. Rapid removal of tetracycline antibiotics from water by coagulation-flotation of sodium dodecyl sulfate and poly (allylamine hydrochloride) in the presence of Al(III) ions. *Sep. Purif. Technol.* 187, 76–83. <https://doi.org/10.1016/j.seppur.2017.06.036>.
- Sales, A., Lima, S.A., 2010. Use of Brazilian sugarcane bagasse ash in concrete as sand replacement. *Waste Manage.* 30 (6), 1114–1122. <https://doi.org/10.1016/j.wasman.2010.01.026>.
- Saosee, P., Sajjakulnukit, B., Gheewala, S.H., 2020. Life cycle assessment of wood pellet production in Thailand. *Sustainability* 12 (17). <https://doi.org/10.3390/su12176996>.
- Sidney Santana, C., Nicodemus Ramos, M.D., Vieira Velloso, C.C., Aguiar, A., 2019. Kinetic evaluation of dye decolorization by Fenton processes in the presence of 3-hydroxyanthranilic acid. *Int. J. Environ. Res. Public Health* 16 (9). <https://doi.org/10.3390/ijerph16091602>.
- Soufi, A., Hajjaoui, H., Elmoubarki, R., Abdennouri, M., Qourzal, S., Barka, N., 2021. Spinel ferrites nanoparticles: Synthesis methods and application in heterogeneous Fenton oxidation of organic pollutants – A review. *Appl. Surf. Sci. Adv.* 6, 100145 <https://doi.org/10.1016/j.apsadv.2021.100145>.
- Subramanian, V., Ordonsky, V.V., Legras, B., Cheng, K., Cordier, C., Chernavskii, P.A., Khodakov, A.Y., 2016. Design of iron catalysts supported on carbon–silica composites with enhanced catalytic performance in high-temperature Fischer-Tropsch synthesis. *Catal. Sci. Technol.* 6 (13), 4953–4961. <https://doi.org/10.1039/C6CY00060F>.
- Šuligoj, A., Trendafilova, I., Maver, K., Pintar, A., Ristić, A., Dražić, G., Abdelraheem, W. H.M., Jagličić, Z., Arčon, I., Logar, N.Z., Dionysiou, D.D., Novak Tušar, N., 2023. Multicomponent Cu-Mn-Fe silica supported catalysts to stimulate photo-Fenton-like water treatment under sunlight. *J. Environ. Chem. Eng.* 11 (5), 110369 <https://doi.org/10.1016/j.jece.2023.110369>.
- Tang, J., Wang, J., 2018. Fenton-like degradation of sulfamethoxazole using Fe-based magnetic nanoparticles embedded into mesoporous carbon hybrid as an efficient catalyst. *Chem. Eng. J.* 351, 1085–1094. <https://doi.org/10.1016/j.jece.2018.06.169>.
- Tao, S., Liang, S., Chen, X., Zhu, Y., Yu, W., Hou, H., Hu, J., Xiao, K., Yuan, S., Yang, J., 2023. Enhanced sludge dewatering by PDMDAAC coupled with Fenton-like reaction initiated by Fe-rich sludge biochar with in-situ generation of H<sub>2</sub>O<sub>2</sub>: Fe/C structure as an electron shuttle. *Resour. Conserv. Recycl.* 198, 107184 <https://doi.org/10.1016/j.resconrec.2023.107184>.
- Thangaraj, B., Jia, Z., Dai, L., Liu, D., Du, W., 2019. Effect of silica coating on Fe<sub>3</sub>O<sub>4</sub> magnetic nanoparticles for lipase immobilization and their application for biodiesel production. *Arab. J. Chem.* 12 (8), 4694–4706. <https://doi.org/10.1016/j.arabjc.2016.09.004>.
- Vinayagam, R., Pai, S., Murugesan, G., Varadavenkatesan, T., Narayanasamy, S., Selvaraj, R., 2022. Magnetic activated charcoal/Fe<sub>2</sub>O<sub>3</sub> nanocomposite for the adsorptive removal of 2,4-dichlorophenoxyacetic acid (2,4-D) from aqueous solutions: Synthesis, characterization, optimization, kinetic and isotherm studies. *Chemosphere* 286, 131938. <https://doi.org/10.1016/j.chemosphere.2021.131938>.
- Wang, C., Sun, R., Huang, R., Wang, H., 2021. Superior fenton-like degradation of tetracycline by iron loaded graphitic carbon derived from microplastics: Synthesis, catalytic performance, and mechanism. *Sep. Purif. Technol.* 270, 118773 <https://doi.org/10.1016/j.seppur.2021.118773>.
- Wang, N., Zheng, T., Zhang, G., Wang, P., 2016. A review on Fenton-like processes for organic wastewater treatment. *J. Environ. Chem. Eng.* 4 (1), 762–787. <https://doi.org/10.1016/j.jece.2015.12.016>.
- Wang, J., Zhuan, R., 2020. Degradation of antibiotics by advanced oxidation processes: An overview. *Sci. Total Environ.* 701, 135023 <https://doi.org/10.1016/j.scitotenv.2019.135023>.
- Webber, C., Jr, P., Spaunhorst, D., Petrie, E. 2017. Impact of sugarcane bagasse ash as an amendment on the physical properties, nutrient content and seedling growth of a certified organic greenhouse growing media. *J. Agric. Sci.* 9, 1, 10.5539/jas.v9n7p1.
- Wu, C., Guo, T., Chen, Y., Tian, Q., Zhang, Y., Huang, Z., Hu, H., Gan, T., 2024. Facile synthesis of excellent Fe<sub>3</sub>O<sub>4</sub>@starch-derived carbon photo-Fenton catalyst for tetracycline degradation: Rapid Fe<sup>3+</sup>/Fe<sup>2+</sup> circulation under visible light condition. *Sep. Purif. Technol.* 329, 125174 <https://doi.org/10.1016/j.seppur.2023.125174>.
- Xiang, Y., Huang, Y., Xiao, B., Wu, X., Zhang, G., 2020. Magnetic yolk-shell structure of ZnFe<sub>2</sub>O<sub>4</sub> nanoparticles for enhanced visible light photo-Fenton degradation towards antibiotics and mechanism study. *Appl. Surf. Sci.* 513, 145820 <https://doi.org/10.1016/j.apsusc.2020.145820>.
- Xu, Q., Ji, T., Gao, S.-J., Yang, Z., Wu, N., 2018. Characteristics and applications of sugar cane bagasse ash waste in cementitious materials. *Mater.* 12, 39. <https://doi.org/10.3390/ma12010039>.
- Yi, Y., Tu, G., Zhao, D., Tsang, P.E., Fang, Z., 2019. Biomass waste components significantly influence the removal of Cr(VI) using magnetic biochar derived from four types of feedstocks and steel pickling waste liquor. *Chem. Eng. J.* 360, 212–220. <https://doi.org/10.1016/j.jcej.2018.11.205>.
- Yoo, S.H., Jang, D., Joh, H.-I., Lee, S., 2017. Iron oxide/porous carbon as a heterogeneous Fenton catalyst for fast decomposition of hydrogen peroxide and efficient removal of methylene blue. *J. Mater. Chem. a* 5 (2), 748–755. <https://doi.org/10.1039/C6TA07457J>.
- Yoon, S., Bae, S., 2019. Novel synthesis of nanoscale zerovalent iron from coal fly ash and its application in oxidative degradation of methyl orange by Fenton reaction. *J. Hazard. Mater.* 365, 751–758. <https://doi.org/10.1016/j.jhazmat.2018.11.073>.
- Zhang, Y., Shi, J., Xu, Z., Chen, Y., Song, D., 2018. Degradation of tetracycline in a schorl/H<sub>2</sub>O<sub>2</sub> system: Proposed mechanism and intermediates. *Chemosphere* 202, 661–668. <https://doi.org/10.1016/j.chemosphere.2018.03.116>.
- Zhu, X., Qian, F., Liu, Y., Matera, D., Wu, G., Zhang, S., Chen, J., 2016. Controllable synthesis of magnetic carbon composites with high porosity and strong acid resistance from hydrochar for efficient removal of organic pollutants: An overlooked influence. *Carbon* 99, 338–347. <https://doi.org/10.1016/j.carbon.2015.12.044>.